ChemPubSoc Europe

DOI: 10.1002/batt.201900079

BATTERIES & SUPERCAPS Communications

A Nonaqueous Na-Ion Hybrid Micro-Supercapacitor with Wide Potential Window and Ultrahigh Areal Energy Density

Panpan Zhang,[a] Lanlan Wang,[a, b] Faxing Wang,[a] Deming Tan,[c] Gang Wang,[a] Sheng Yang,[a] Minghao Yu,[a] Jian Zhang,*[a] and Xinliang Feng*[a]

The increasing demand on smart miniaturized electronics has greatly boosted the development of high-performance micro-supercapacitors (MSCs). However, the unsatisfied electrochemical performance (e.g., narrow potential window, low areal energy density) impedes their wide applications. Here, we demonstrate a novel type of nonaqueous Na-ion hybrid MSC, using VS_2 nanosheets grown on electrochemically exfoliated graphene (VS_2@EG) as the negative electrode and activated carbon as the positive electrode in nonaqueous sodium-ion electrolyte. Such constructed nonaqueous Na-ion hybrid MSCs show a remarkable areal capacitance of 110.7 mF cm^{-2} at 0.2 mA cm^{-2} in a wide potential range of 0.01–3.5 V and an outstanding areal energy density of 188.3 μWh cm^{-2}. Besides, an impressive cycling stability up to 5000 cycles without noticeable decay is also achieved for the nonaqueous Na-ion hybrid MSCs. This new hybrid MSC holds great potential application in on-chip electronics.

Increasing interests in on-chip electronic devices have significantly stimulated the growing demand for low-cost and high-performance miniaturized energy power sources.[1] Among them, micro-supercapacitors (MSCs), have attracted much attention due to their intrinsic advantages such as high power densities, fast charge/discharge rates, and long operating cycles.[2] However, the recently reported MSCs still suffer from the poor overall electrochemical performance, especially narrow potential window and low areal energy density.[3]

To overcome the aforementioned challenges, nonaqueous hybrid MSCs represent a good solution by coupling a capacitor-type cathode and a battery-type anode with expanded operating voltage and enhanced energy density.[4] Among them, the Na-ion hybrid MSC is a promising candidate due to the large accessibility of low-cost Na and electrolyte.[5] Currently, the reaction kinetics of the anode electrodes (e.g., $Na_2Ti_3O_7$,[6] V_2O_5,[7] TiO_2,[8] Li_3VO_4,[9] *etc.*) based on a diffusion-controlled intercalation process (i.e. conversion or alloying) are much slower than those of the cathode electrodes (e.g., activated carbon,[10] carbon nanotubes,[11] graphene,[12] etc.) based on a surface-controlled process. As an emerging member of transitional metal dichalcogenides, VS_2 has been widely applied in electrochemical energy storage devices owing to many intriguing chemical and physical properties.[13] However, its potential in nonaqueous Na-ion hybrid MSC is underexplored.

In this work, we constructed a new-type nonaqueous Na-ion hybrid MSC with wide potential window and ultrahigh areal energy density by using activated carbon (AC), vertically aligned VS_2 nanosheets on electrochemically exfoliated graphene (VS_2@EG) sheets, and nonaqueous $NaClO_4$ dispersion serving as cathode, anode, and electrolyte, respectively. Notably, ion adsorption/desorption on the AC electrode and surface-controlled process on the VS_2@EG electrode enable the constructed Na-ion hybrid MSCs presenting a high reversiblity during charge/discharge process with a wide voltage range of 0.01-3.5 V. As a result, the areal capacitance reaches 110.7 mF cm^{-2} at 0.2 mA cm^{-2} and the areal energy density can be as high as 188.3 μWh cm^{-2} at 0.35 mW cm^{-2}, by far outperforming the recently reported MSCs. Furthermore, the as-fabricated nonaqueous Na-ion hybrid MSCs exhibit an excellent cyclability of up to 5000 cycles without capacitance fading.

The detailed fabrication procedure of nonaqueous Na-ion hybrid MSCs is described in the Experimental Section of Supporting Information (Figure S1–4). Specially, the slurry comprised of active materials (VS_2@EG or AC), binder, and conductive carbon black was formed and transferred into the pre-patterned channels as the anode or cathode electrode with the asymmetric configuration (Figure 1a). The solution of $NaClO_4$ (1 M) dissolved in the mixture of ethylene carbonate and diethyl carbonate (volume ratio of 1:1) with 5 wt% fluoroethylene carbonate (FEC) was used as the organic electrolyte. FEC was added for the formation of a protective solid electrolyte interface layer. After casting the electrolyte onto the

[a] P. Zhang, Dr. L. Wang, F. Wang, Dr. G. Wang, Dr. S. Yang, Dr. M. Yu, Dr. J. Zhang, Prof. X. Feng
Department of Chemistry and Food Chemistry &
Center for Advancing Electronics Dresden (cfaed)
Technische Universität Dresden
01062 Dresden, Germany
E-mail: jian.zhang1@tu-dresden.de
xinliang.feng@tu-dresden.de

[b] Dr. L. Wang
State Key Laboratory for Manufacturing Systems Engineering
School of Mechanical Engineering
Xi'an Jiaotong University
Xi'an 710054, China

[c] D. Tan
Department of Chemistry and Food Chemistry
Technische Universität Dresden
01069 Dresden, Germany

Supporting information for this article is available on the WWW under https://doi.org/10.1002/batt.201900079

This publication is part of a joint Special Collection with ChemSusChem focusing on "2D Energy Storage Materials".

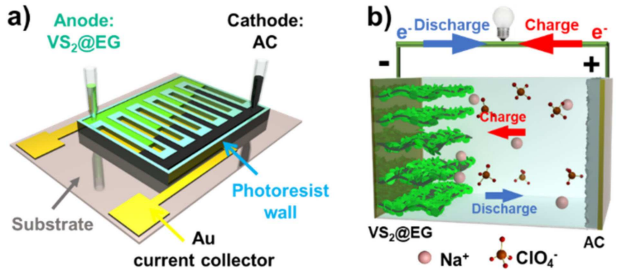

Figure 1. a) Schematic illustration of the asymmetric configuration of non-aqueous Na-ion hybrid MSCs by transferring the slurry consisting of VS_2@EG (or AC), binder, and acetylene black into the pre-patterned microchannels. b) Working mechanism of nonaqueous Na-ion hybrid MSCs.

interdigital electrode, the device was covered with plastic film and sealed by the UV-curing optical adhesive in an argon-filled glovebox. The resultant Na-ion hybrid MSC is with the total size of 2×2 cm^2 (Figure S5).

The synthetic procedure of VS_2@EG electrode is based on the prior-fabrication of high-quality EG sheets and followed by hydrothermal growth of vertically aligned VS_2 nanosheets on both sides of EG sheets. EG sheets were fabricated according to our previous reports using an electrochemical exfoliation of graphite.[14] They have lateral dimension (1-5 μm), low defect density (C/O ratio of 16.4) (Figure S6, 7), and high electrical conductivity (1.26 kΩ q^{-1}), which render them as the ideal building unit to construct 2D hybrids. The growing process of VS_2 nanosheets on EG was inspected by the scanning electron microscope (SEM) characterizations at different growth times (Figure S8). During the growing process, L-cysteine gradually decomposed and released H_2S to react with the vanadium precursor. At the early nucleation stage, many small VS_2 branches formed on the both sides of EG. With increasing the reaction time, these nanoflakes expanded along their basal planes, then transformed to ultrathin nanosheets and eventually formed the hierarchical VS_2 nanostructure. Due to the matched surface energy and low viscosity, NMP as hydrothermal solvent was used to preserve the nanostructure and suppress the aggregation of VS_2@EG. As shown in Figure 2a–c, VS_2@EG displayed typical 2D morphology anchored on both sides with shell-like wrinkled VS_2 nanosheets with an average lateral size of 200 nm and thickness of 7 nm. The successful growth of VS_2 alleviates the restacking of EG sheets. The distribution of the elements in VS_2@EG was manifested by energy-dispersive spectroscopy (EDS) elemental mapping analysis. It is proved that C, S, and V elements were homogeneously distributed within the 2D hybrids (Figure 2d). Additionally, the vertical alignment of VS_2 nanosheets on EG sheets was investigated by high-resolution transmission electron micro-

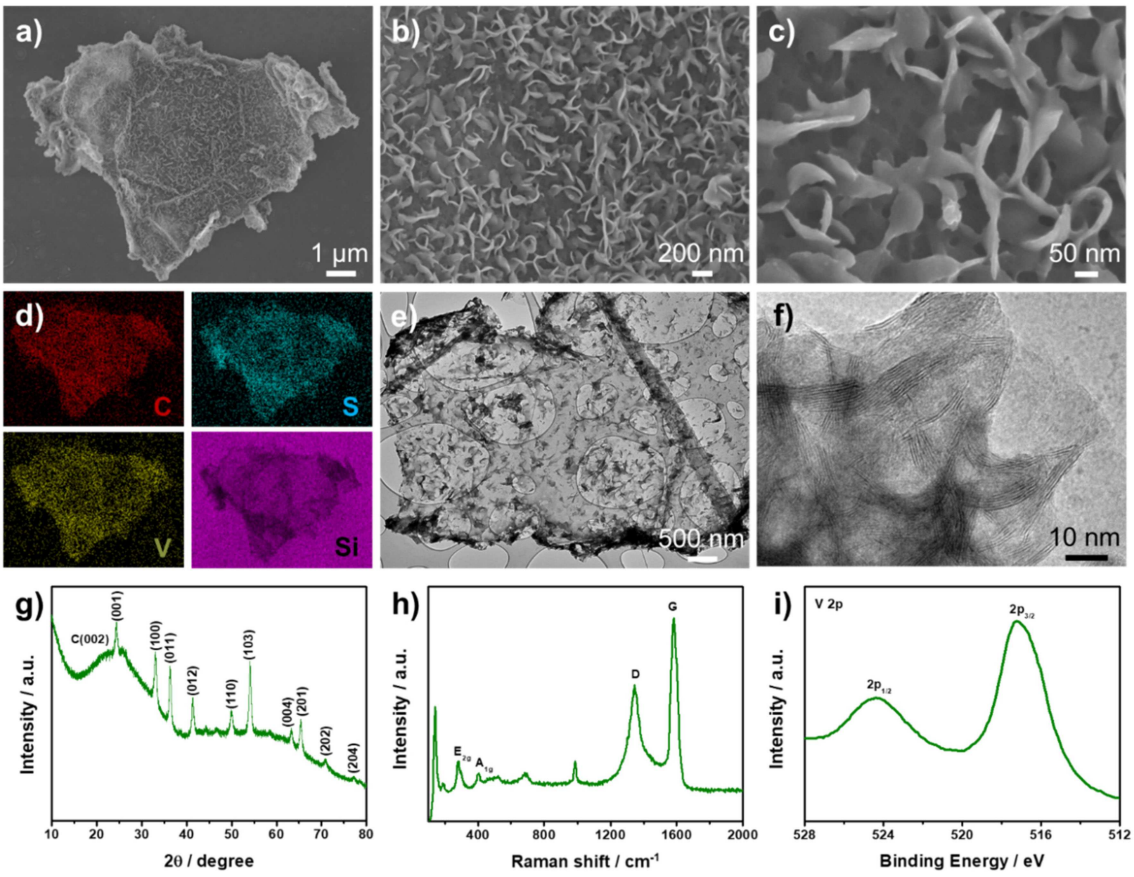

Figure 2. Morphological and structural characterizations of VS_2@EG electrode. a-d) SEM images with different magnifications and corresponding elemental mapping analysis. e,f) HRTEM images with different magnifications. g) XRD pattern, h) Raman spectrum, and i) XPS spectrum of VS_2@EG.

scope (HRTEM) images, as depicted in Figure 2e,f, where each VS_2 nanosheets contained ~10 atomic layers.

The structural characterizations of the synthesized VS_2@EG were further inspected by X-ray diffraction (XRD), Raman spectroscopy, and X-ray photoelectron spectroscopy (XPS). The XRD pattern in Figure 2g indicates the typical crystal domains with a hexagonal structure, where the diffraction peaks match well with the standard VS_2 (JCPDS card No. 89-1640).[13d,15] Raman spectrum of VS_2@EG (Figure 2h) illustrates the E_{2g}, A_{1g} vibration modes of VS_2 as well as D and G bands of EG, respectively. Additionally, as shown in Figure 2i and Figure S9, XPS spectra further confirm the presence of V, S, C, and O elements in VS_2@EG. The weight ratio of EG in the 2D hybrids was estimated to be 14.7 wt% based on the thermogravimetric analysis (Figure S10).

The hierarchical structure with fully exposed VS_2 nanosheets and conductive EG substrates makes VS_2@EG a promising anode material for Na-ion storage. The electrochemical property of VS_2@EG anode was firstly assessed in half cells. Na foil was used as both the counter and reference electrodes. The galvanostatic charge-discharge (GCD) profiles of the VS_2@EG anode present two voltage plateaus (Figure 3a), consistent with the CV curves in Figure 3c. In detail, when the cathodic scan occurred, two main peaks were observed at 1.43 and 0.46 V, indicating the phase transitions with Na^+ insertion.[13d] While turning to the anodic scan, there were two peaks located at 1.62 and 1.96 V, corresponding to the slight working plateaus. The multi-step reaction during Na^+ intercalation-de-intercalation processes can be ascribed to the formation of various Na/vacancy ordered patterns as a function of Na content.[15d] The specific capacitance of the VS_2@EG is calculated to be 407 $F g^{-1}$ at 0.2 $A g^{-1}$ and it maintained at 348 $F g^{-1}$ even at a high current density of 1.6 $A g^{-1}$ (Figure 3b). Cyclic voltammetry (CV) measurement from 0.5 to 8 $mV s^{-1}$ (Figure 3c) was also performed to calculate the pseudocapacitive contribution to the total capacitance in VS_2@EG. Notably, the VS_2@EG electrode delivered a higher impressive current density in comparison with those of pure EG and VS_2 electrodes at 5 $mV s^{-1}$ (Figure S11), proving the much improved capacitance due to the synergistic effect. The change in peak current (*i*, A) with the

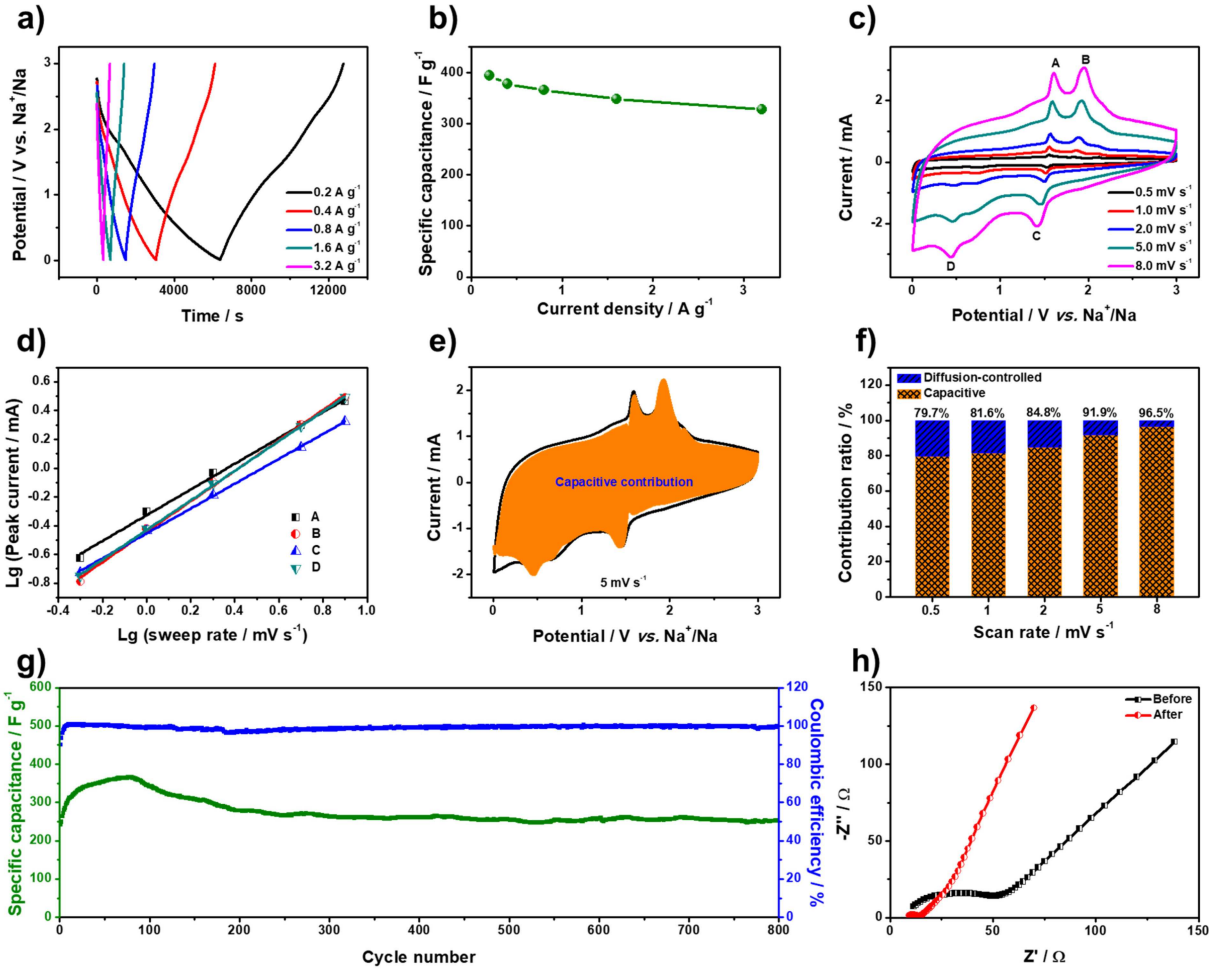

Figure 3. Electrochemical performance of VS_2@EG as anode material in half cells. a) GCD curves at current densities of 0.2–3.2 $A g^{-1}$. b) Specific capacitances calculated from GCD curves as a function of current density. c) CV profiles at various scan rates from 0.5 to 8 $mV s^{-1}$. d) Log *i* versus log *v* plots at each redox peak. e) CV curve of VS_2@EG with separation between the total current and the capacitive (orange) current at 5 $mV s^{-1}$. f) Normalized contribution ratios of the capacitive (orange) and diffusion-controlled (blue) components as a function of scan rate. g) Cycling performance of the fabricated VS_2@EG at 3.2 $A g^{-1}$ and h) Nyquist plots before and after 800 GCD cycles.

sweep rate (v, mV s^{-1}) can be generally expressed as $i = av^b$.[16] Particularly, the b value of 0.5 means a diffusion-controlled redox reaction, whereas that of 1.0 suggests a surface-controlled or capacitive process. Here, b-values of the four redox peaks (A, B, C, and D) were determined to be 0.9, 1, 0.9, and 1 (Figure 3d), indicating a dominant capacitive behavior of VS_2@EG during the electrochemical reactions. Kinetic analysis was carried out to confirm the redox pseudocapacitance-like contribution in the CV profiles. The total current (i) is divided into two parts according to the equation: $i = k_1v + k_2v^{1/2}$, where k_1v means the capacitive effect and $k_2v^{1/2}$ corresponds to the diffusion-controlled contribution.[17] The pseudocapacitive fraction of the total charge is 91.9% at a scan rate of 5 mV s^{-1} (Figure 3e). Moreover, the percentages of pseudocapacitive and diffusion-controlled contributions at various scan rates are summarized in Figure 3f. The pseudocapacitive contribution reaches a maximum value (96.5%) at the highest sweep rate of 8 mV s^{-1} with an increase of scan rate. This result clearly suggests that VS_2@EG offers exposed active surface sites for the fast Na^+ insertion/extraction and good rate capability due to the hierarchical porous structure. In addition, when charging/discharging at the current density over 800 cycles (Figure 3g), VS_2@EG did not show noticeable capacitance decay with an average coulombic efficiency of 99%. According to the electrochemical impedance spectra (EIS) during the cycling measurement, the much smaller semicircle at high and middle frequencies means the decreased charge transfer resistance, indicating the full availability of the electrode surface for reversible ionic intercalation (Figure 3h). In the low frequency range, the straight line of VS_2@EG electrode with larger slope after the cycling suggests the enhanced mass transfer inside electrode materials. The insertion of sodium into the VS_2 during the cycling measurement significantly improves the electronic conductivity of the whole electrode.[13g,18]

Next, the Na-ion hybrid MSC was thus assembled based on VS_2@EG and AC electrodes in a $NaClO_4$-contained organic electrolyte (Figure 1b). A proper mass balance between the two electrodes was carried out to attain a high efficiency. According to the above-mentioned electrochemical behavior of VS_2@EG anode and AC cathode against Na foil in half cells, the ideal mass ratio of AC/VS_2@EG was determined in the range of 3.4–4. The average total weight of VS_2@EG anode and AC cathode is about 3 mg. The thicknesses of VS_2@EG and AC electrodes in assembled Na-ion hybrid MSCs are around 10 and 40 μm, respectively (Figure S17, 18). The voltage of the nonaqueous Na-ion hybrid MSC reached 3.5 V (Figure 4a). Figure 4b displays the GCD profiles at different current densities and the asymmetric shapes are typical features below to pseudocapacitive charge storage behavior. One charge–discharge process for the nonaqueous Na-ion hybrid MSC took 2400 seconds to complete at a current density of 0.2 mA cm^{-2}, resulting in an impressive areal capacitance of 110.7 mF cm^{-2} (Figure 4b). Upon increasing the current density to 1 mA cm^{-2}, its areal capacitance still remained at 58.5 mF cm^{-2} (Figure 4c). Moreover, the areal capacitance up to 5000 cycles did not show any noticeable capacitance fading at 1 mA cm^{-2} (Figure 4d). Interestingly, there was even a slight increase of the areal capacitance, which can be attributed to the increasing wetting ability of the microelectrodes by the electrolyte. Additionally, postmortem SEM and corresponding EDS mapping analysis were performed before and after cycling (Figure S19–22). The preservation of morphology and composition indicated good stability of VS_2@EG anode and AC cathode. Figure 4e shows the EIS of nonaqueous Na-ion hybrid MSCs during the cycling

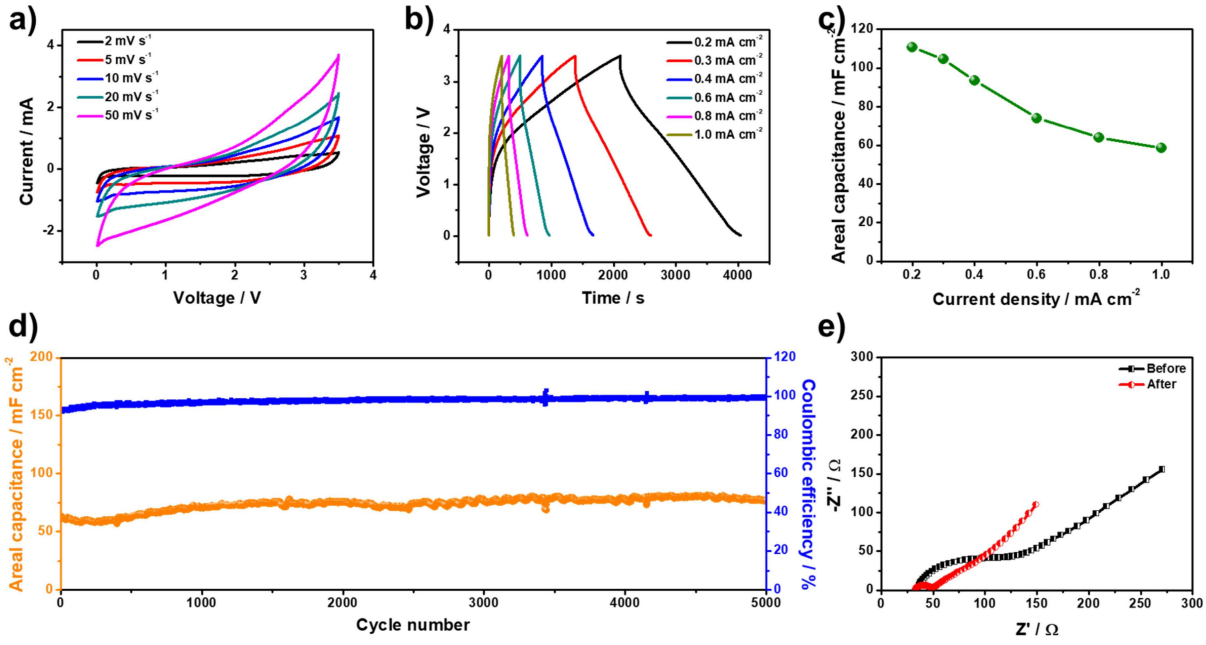

Figure 4. Electrochemical performance of nonaqueous Na-ion hybrid MSCs. a) CV curves at scan rates of 2–50 mV s^{-1}. b) GCD curves at the current densities ranging from 0.2 to 1.0 mA cm^{-2}. c) Areal capacitances as a function of current density. d) Cycling performance of the Na-ion hybrid MSCs at 1 mA cm^{-2} and e) Nyquist plots before and after 5000 GCD cycles.

measurements. The semicircle at the high frequency denotes charge transfer resistance (R_{ct}) in correlation with reaction kinetics, while the slope at the low frequency represents Na^+ diffusion behaviors inside electrode materials. The decrease of R_{ct} from 110.7 to 49.2 Ω after cycling testing suggests an improved reaction kinetic of nonaqueous Na-ion hybrid MSCs, matching well with the enhanced capacitance after cycling test.[19]

Owing to the limited space of miniaturized devices, the electrochemical performance per areas are considerable than the values calculated per mass or volume.[3a,20] Consequently, to verify the outstanding performance of the nonaqueous Na-ion hybrid MSCs, the areal energy and power densities of recently reported MSCs are summarized in Ragone plots for comparison (Figure 5). Remarkably, such Na-ion hybrid MSCs exhibit much

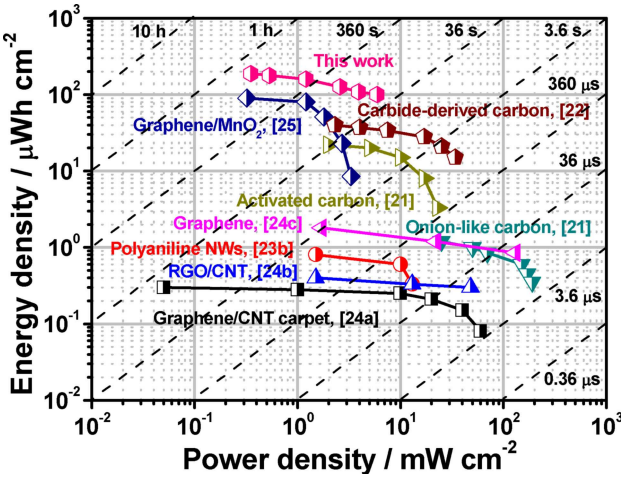

Figure 5. Ragone plots showing areal energy and power densities of nonaqueous Na-ion hybrid MSCs in comparison with other typically reported MSCs.

higher areal energy density of 188.3 µWh cm^{-2} at 0.35 mW cm^{-2}, superior to those of other previous MSCs including onion-like carbon,[21] carbide-derived carbon,[22] AC,[21] polyaniline nanowire,[23] graphene,[19b,24] and graphene/MnO_2.[25] What's more, the nonaqueous Na-ion hybrid MSC presents an excellent power density of 5.9 mW cm^{-2} at 99.7 µWh cm^{-2}, well comparable to most reported MSCs using carbon materials.[24] As shown in Table S1, the overall electrochemical performance of our hybrid device is able to compete with microbatteries and electrolytic capacitors for diverse energy applications.

In summary, we demonstrated the synthesis of pseudocapacitive VS_2@EG anode material for constructing new-type nonaqueous Na-ion hybrid MSCs with high operating voltage window (0.01–3.5 V) in a $NaClO_4$-contained organic electrolyte. The assembled nonaqueous Na-ion hybrid MSCs delivered a rather high areal capacitance of 110.7 mF cm^{-2} at 0.2 mA cm^{-2} and outstanding areal energy density of 188.3 µWh cm^{-2} at the power density of 0.35 mW cm^{-2}. It can be charged and discharged for 5000 times without capacitance retention, attributed to the asymmetric design of pseudocapacitive VS_2@EG anode and electric double layer-type AC cathode. Thus, this work not only promotes the development of new miniaturized energy storage devices, but also implies a great potential in future self-powered electronics.

Acknowledgements

This work is financially supported by the Initiative and Networking Fund of the German Helmholtz Association, Helmholtz International Research School for Nanoelectronic Networks NanoNet (VH-KO-606), the European Union's Horizon 2020 research and innovation programme under grant agreement No 785219. We gratefully acknowledge the Center of Advancing Electronics Dresden (cfaed) and Dresden Center for Nanoanalysis (DCN) at TU Dresden.

Conflict of Interest

The authors declare no conflict of interest.

Keywords: nonaqueous · Na-ion · hybrid micro-supercapacitor · potential window · energy density

[1] a) Y. Liu, K. He, G. Chen, W. R. Leow, X. Chen, *Chem. Rev.* **2017**, *117*, 12893; b) J. Li, J. Zhao, J. A. Rogers, *Acc. Chem. Res.* **2019**, *52*, 53; c) L. Wang, K. Wang, Z. Lou, K. Jiang, G. Shen, *Adv. Funct. Mater.* **2018**, *28*, 1804510; d) C. Wang, K. Xia, H. Wang, X. Liang, Z. Yin, Y. Zhang, *Adv. Mater.* **2019**, *31*, 1801072; e) P. Zhang, F. Wang, M. Yu, X. Zhuang, X. Feng, *Chem. Soc. Rev.* **2018**, *47*, 7426.
[2] a) C. Lethien, J. Le Bideau, T. Brousse, *Energy Environ. Sci.* **2019**, *12*, 96; b) S. Zheng, X. Shi, P. Das, Z. S. Wu, X. Bao, *Adv. Mater.* **2019**, *31*, 1900583; c) F. Wang, X. Wu, X. Yuan, Z. Liu, Y. Zhang, L. Fu, Y. Zhu, Q. Zhou, Y. Wu, W. Huang, *Chem. Soc. Rev.* **2017**, *46*, 6816; d) G. Xiong, C. Meng, R. G. Reifenberger, P. P. Irazoqui, T. S. Fisher, *Electroanalysis* **2014**, *26*, 30.
[3] a) M. Beidaghi, Y. Gogotsi, *Energy Environ. Sci.* **2014**, *7*, 867; b) N. Liu, Y. Gao, *Small* **2017**, *13*, 1701989; c) L. Liu, Z. Niu, J. Chen, *Nano Res.* **2017**, *10*, 1524.
[4] a) Y. Shao, M. F. El-Kady, J. Sun, Y. Li, Q. Zhang, M. Zhu, H. Wang, B. Dunn, R. B. Kaner, *Chem. Rev.* **2018**, *118*, 9233; b) N. Choudhary, C. Li, J. Moore, N. Nagaiah, L. Zhai, Y. Jung, J. Thomas, *Adv. Mater.* **2017**, *29*, 1605336; c) H. Wang, C. Zhu, D. Chao, Q. Yan, H. J. Fan, *Adv. Mater.* **2017**, *29*, 1702093; d) J. Ding, W. Hu, E. Paek, D. Mitlin, *Chem. Rev.* **2018**, *118*, 6457; e) W. Zuo, R. Li, C. Zhou, Y. Li, J. Xia, J. Liu, *Adv. Sci.* **2017**, *4*, 1600539; f) V. Aravindan, M. Ulaganathan, S. Madhavi, *J. Mater. Chem. A* **2016**, *4*, 7538.
[5] B. D. Boruah, *Energy Storage Mater.* **2019**, DOI: 10.1016/j.ensm.2019.06.012.
[6] H. Li, L. Peng, Y. Zhu, X. Zhang, G. Yu, *Nano Lett.* **2016**, *16*, 5938.
[7] Z. Chen, V. Augustyn, X. Jia, Q. Xiao, B. Dunn, Y. Lu, *ACS Nano* **2012**, *6*, 4319.
[8] Z. Le, F. Liu, P. Nie, X. Li, X. Liu, Z. Bian, G. Chen, H. B. Wu, Y. Lu, *ACS Nano* **2017**, *11*, 2952.
[9] L. Shen, H. Lv, S. Chen, P. Kopold, P. A. van Aken, X. Wu, J. Maier, Y. Yu, *Adv. Mater.* **2017**, *29*, 1700142.
[10] P. Jeżowski, O. Crosnier, E. Deunf, P. Poizot, F. Béguin, T. Brousse, *Nat. Mater.* **2017**, *17*, 167.
[11] a) W. Zuo, C. Wang, Y. Li, J. Liu, *Sci. Rep.* **2015**, *5*, 7780; b) P. Zhang, X. Zhao, Z. Liu, F. Wang, Y. Huang, H. Li, Y. Li, J. Wang, Z. Su, G. Wei, Y. Zhu, L. Fu, Y. Wu, W. Huang, *NPG Asia Mater.* **2018**, *10*, 429.
[12] F. Zhang, T. Zhang, X. Yang, L. Zhang, K. Leng, Y. Huang, Y. Chen, *Energy Environ. Sci.* **2013**, *6*, 1623.

[13] a) T. M. Masikhwa, F. Barzegar, J. K. Dangbegnon, A. Bello, M. J. Madito, D. Momodu, N. Manyala, *RSC Adv.* **2016**, *6*, 38990; b) B. Pandit, L. K. Bommineedi, B. R. Sankapal, *J. Energy Chem.* **2019**, *31*, 79; c) X. Ou, X. Liang, F. Zheng, Q. Pan, J. Zhou, X. Xiong, C. Yang, R. Hu, M. Liu, *Chem. Eng. J.* **2017**, *320*, 485; d) D. Yu, Q. Pang, Y. Gao, Y. Wei, C. Wang, G. Chen, F. Du, *Energy Storage Mater.* **2018**, *11*, 1; e) M. N. Rantho, M. J. Madito, F. O. Ochai-Ejeh, N. Manyala, *Electrochim. Acta* **2018**, *260*, 11; f) Q. Ji, C. Li, J. Wang, J. Niu, Y. Gong, Z. Zhang, Q. Fang, Y. Zhang, J. Shi, L. Liao, X. Wu, L. Gu, Z. Liu, Y. Zhang, *Nano Lett.* **2017**, *17*, 4908; g) R. Sun, Q. Wei, Q. Li, W. Luo, Q. An, J. Sheng, D. Wang, W. Chen, L. Mai, *ACS Appl. Mater. Interfaces* **2015**, *7*, 20902; h) X. Zhu, W. Zhao, Y. Song, Q. Li, F. Ding, J. Sun, L. Zhang, Z. Liu, *Adv. Energy Mater.* **2018**, *8*, 1800201; i) N. A. Kalam, C. Sengottaiyan, R. Jayavel, K. Ariga, R. G. Shrestha, T. Subramani, S. Sankar, L. K. Shrestha, *J. Taiwan Inst. Chem. E.* **2018**, *92*, 72; j) J. Feng, X. Sun, C. Wu, L. Peng, C. Lin, S. Hu, J. Yang, Y. Xie, *J. Am. Chem. Soc.* **2011**, *133*, 17832.

[14] a) K. Parvez, Z.-S. Wu, R. Li, X. Liu, R. Graf, X. Feng, K. Müllen, *J. Am. Chem. Soc.* **2014**, *136*, 6083; b) S. Yang, M. R. Lohe, K. Müllen, X. Feng, *Adv. Mater.* **2016**, *28*, 6213; c) Z. S. Wu, K. Parvez, S. Li, S. Yang, Z. Liu, S. Liu, X. Feng, K. Müllen, *Adv. Mater.* **2015**, *27*, 4054.

[15] a) J. Zhou, L. Wang, M. Yang, J. Wu, F. Chen, W. Huang, N. Han, H. Ye, F. Zhao, Y. Li, Y. Li, *Adv. Mater.* **2017**, *29*, 1702061; b) P. He, M. Yan, G. Zhang, R. Sun, L. Chen, Q. An, L. Mai, *Adv. Energy Mater.* **2017**, *7*, 1601920; c) R. Sun, Q. Wei, J. Sheng, C. Shi, Q. An, S. Liu, L. Mai, *Nano Energy* **2017**, *35*, 396; d) E. Lee, S. Sahgong, C. S. Johnson, Y. Kim, *Electrochim. Acta* **2014**, *143*, 272.

[16] a) V. Augustyn, J. Come, M. A. Lowe, J. W. Kim, P.-L. Taberna, S. H. Tolbert, H. D. Abruña, P. Simon, B. Dunn, *Nat. Mater.* **2013**, *12*, 518; b) G. Wang, J. Zhang, S. Yang, F. Wang, X. Zhuang, K. Müllen, X. Feng, *Adv. Energy Mater.* **2018**, *8*, 1702254.

[17] T. Brezesinski, J. Wang, S. H. Tolbert, B. Dunn, *Nat. Mater.* **2010**, *9*, 146.

[18] a) K. Zou, P. Cai, C. Liu, J. Li, X. Gao, L. Xu, G. Zou, H. Hou, Z. Liu, X. Ji, *J. Mater. Chem. A* **2019**, *7*, 13540; b) S. Wang, F. Gong, S. Yang, J. Liao, M. Wu, Z. Xu, C. Chen, X. Yang, F. Zhao, B. Wang, Y. Wang, X. Sun, *Adv. Funct. Mater.* **2018**, *28*, 1801806; c) J. Wang, N. Luo, J. Wu, S. Huang, L. Yu, M. Wei, *J. Mater. Chem. A* **2019**, *7*, 3691.

[19] a) P. Zhang, J. Wang, W. Sheng, F. Wang, J. Zhang, F. Zhu, X. Zhuang, R. Jordan, O. G. Schmidt, X. Feng, *Energy Environ. Sci.* **2018**, *11*, 1717; b) P. Zhang, F. Zhu, F. Wang, J. Wang, R. Dong, X. Zhuang, O. G. Schmidt, X. Feng, *Adv. Mater.* **2017**, *29*, 1604491.

[20] N. A. Kyeremateng, T. Brousse, D. Pech, *Nat. Nanotechnol.* **2017**, *12*, 7.

[21] D. Pech, M. Brunet, H. Durou, P. Huang, V. Mochalin, Y. Gogotsi, P.-L. Taberna, P. Simon, *Nat. Nanotechnol.* **2010**, *5*, 651.

[22] P. Huang, C. Lethien, S. Pinaud, K. Brousse, R. Laloo, V. Turq, M. Respaud, A. Demortière, B. Daffos, P. L. Taberna, B. Chaudret, Y. Gogotsi, P. Simon, *Science* **2016**, *351*, 691.

[23] a) K. Wang, W. Zou, B. Quan, A. Yu, H. Wu, P. Jiang, Z. Wei, *Adv. Energy Mater.* **2011**, *1*, 1068; b) C. Z. Meng, J. Maeng, S. W. M. John, P. P. Irazoqui, *Adv. Energy Mater.* **2014**, *4*, 1301269.

[24] a) J. Lin, C. Zhang, Z. Yan, Y. Zhu, Z. Peng, R. H. Hauge, D. Natelson, J. M. Tour, *Nano Lett.* **2013**, *13*, 72; b) M. Beidaghi, C. Wang, *Adv. Funct. Mater.* **2012**, *22*, 4501; c) M. F. El-Kady, R. B. Kaner, *Nat. Commun.* **2013**, *4*, 1475.

[25] M. F. El-Kady, M. Ihns, M. Li, J. Y. Hwang, M. F. Mousavi, L. Chaney, A. T. Lech, R. B. Kaner, *Proc. Natl. Acad. Sci. USA* **2015**, *112*, 4233.

Manuscript received: June 19, 2019
Revised manuscript received: July 22, 2019
Accepted manuscript online: August 5, 2019
Version of record online: August 12, 2019